

Random Matrix Theory Approach to Chaotic Coherent Perfect Absorbers

Huanan Li¹, Suwun Suwunnarat¹, Ragnar Fleischmann², Holger Schanz³, and Tsampikos Kottos¹

¹*Department of Physics, Wesleyan University, Middletown, Connecticut 06459, USA*

²*Max Planck Institute for Dynamics and Self-organization (MPIDS), 37077 Göttingen, Germany and*

³*Institute for Mechanical Engineering, Hochschule Magdeburg-Stendal, 39114 Magdeburg, Germany*

(Dated: February 20, 2022)

We employ Random Matrix Theory in order to investigate coherent perfect absorption (CPA) in lossy systems with complex internal dynamics. The loss strength γ_{CPA} and energy E_{CPA} , for which a CPA occurs are expressed in terms of the eigenmodes of the isolated cavity – thus carrying over the information about the chaotic nature of the target – and their coupling to a finite number of scattering channels. Our results are tested against numerical calculations using complex networks of resonators and chaotic graphs as CPA cavities.

Introduction – Perfect absorption is an interdisciplinary topic relevant for a broad range of technologies, extending from acoustics [1–4] and electronic circuits [5–7], to radio frequencies (RF) [8, 9], microwaves [10–13] and optical frequencies [14–26]. The potential applications range from energy conversion, photovoltaics and imaging, to time-reversal technologies, sensing and soundproofing. In many of these applications, either due to cost or design considerations, the requirement is to achieve maximal absorption from minimal built-in losses. For this goal, new schemes have been devised that exploit spatial arrangements of losses, or utilize novel interferometric protocols. One such approach, called the Coherent Perfect Absorber (CPA) [16], was recently proposed based on a time-reversed laser concept.

A CPA is a *weakly* lossy cavity which acts as a perfect constructive interference trap for incident radiation at a particular frequency and spatial field distribution. This distribution is the time reversal of a lasing mode which the cavity would emit, if the lossy medium is replaced by a gain of equal strength. Since the outgoing signal is null due to the destructive interferences between various pathways, the incoming waves are eventually absorbed even in cases when a weak absorptive mechanism is employed. What makes this approach attractive is the recent developments in wavefront shaping of an incident wave [27–29]. Despite all interest, the existing studies on CPA involve only simple cavities [1, 3, 4, 7, 10, 16–26]. Such CPA cavities have been realized recently in a number of experimental set-ups, ranging from optical to RF and acoustic systems [4, 7, 18].

In this paper we investigate CPA in a new set-up associated with single chaotic cavities or complex networks of cavities coupled to the continuum with multiple channels. The underlying complex classical dynamics of these systems leads to complicated wave interferences that give rise to universal statistical properties of their transport characteristics. A powerful theoretical approach based on Random Matrix Theory (RMT) has been developed and it has been shown that it accurately describes many aspects of such wave chaotic systems, including the structure and statistics of spectra and eigenstates or the dis-

tribution of transmittance, delay times, etc [30–36].

Motivated by this success, we have used an RMT approach to derive expressions for the energy E_{CPA} and loss-strength γ_{CPA} and quantify the sensitivity of CPA on the energy and loss-strength detuning. We have also studied the statistics of (re-scaled) γ_{CPA} , thus providing a guidance for an optimal loss-strength window for which a chaotic CPA can be realized with high probability. Our modeling allows the possibility of spatially non-uniform absorption which might even be localized at a single position. This feature is relevant for recent metamaterial proposals which advocate for the novelty of structures with spatially non-uniform losses (or/and gain) and can be easily realized in set-ups like the ones shown in the insets of Fig. 1 below. Our results are expressed in terms of the modes of the isolated and lossless system which contain the information about the (chaotic) dynamics. Specifically we find that γ_{CPA} depends on a ratio of the absolute-value-squares of eigenmode amplitudes at the boundary and in the absorbing regions of the system. The averaging over the statistics of eigenmode components results in non-trivial distributions which differ qualitatively from the well-known resonance distributions. We have tested the RMT results against numerical data from actual chaotic systems with non-trivial underlying dynamics, namely quantum graphs (Fig. 1b) [37–40]. These models of wave chaos have been already realized in the microwave regime [41–43]. Losses can be included in a controllable manner [44] while a detailed control of the incoming waves in a multi-channel setting can be achieved via IQ-modulators [45]. While in this contribution we concentrated on chaotic CPA traps, our approach can also serve as a basis for RMT modeling of CPA disordered diffusive cavities and CPA cavities with Anderson localization.

RMT modeling and complex cavity networks – The Hamiltonian that describes the isolated (i.e. in the absence of scattering channels) system is modeled by an ensemble of $N \times N$ random matrices H_0 with an appropriate symmetry: in the case that the isolated set-up is time-reversal invariant (TRI), H_0 is taken from a Gaussian Orthogonal Ensemble (GOE), while in the case of

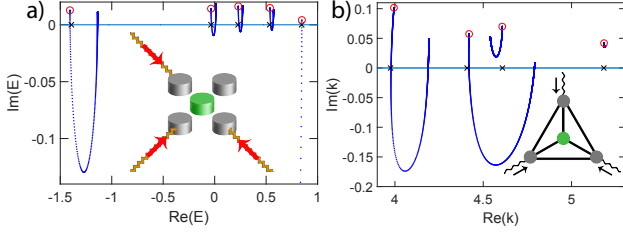


FIG. 1: (color online) (a) Parametric evolution of the complex energy zeros of the scattering matrix for a random network of $N = 5$ cavities and $M = 3$ as γ (green cavity, see inset) increases. The coupling to the leads is $w/t_L = 0.15$ and the matrix elements of H_0 are taken from a box distribution $[-0.5, 0.5]$. At γ_{CPA} the zeros cross the real axis i.e. $(\text{Re}(E), \text{Im}(E)) = (E_{\text{CPA}}, 0)$. The red circles indicate the zeros at $\gamma = 0$ while the crosses indicate the eigenmodes $E_n^{(0)}$ of the isolated system H_0 . (b) The same (in the complex k plane) for a tetrahedron with $N = 4$ vertices, $M = 3$ leads and a lossy vertex (green, see inset) in the middle. The lossless vertices have vertex potential $\lambda\bar{l} = 4\pi$. The bond lengths are taken from a box distribution $[0.5, 1.5]$.

broken TRI it is taken from a Gaussian Unitary Ensemble (GUE) [55]. Such modeling describes (in the coupled mode approximation [46]) complex networks of N coupled cavities, see inset of Fig. 1. The distances between the cavities are random, leading to random couplings. In this case TRI can be violated via magneto-optical effects. Another physical system that is described by our modeling is a set of coupled acoustic chambers or a network of random LC(R) elements. In the latter case the TRI can be violated via a gyrator [47].

Consider now that some of the cavities contain a lossy material. In this case the Hamiltonian H of the isolated system is non-Hermitian and can be modeled as

$$H = H_0 - \iota\Gamma; \quad \Gamma = \sum_{\mu} \gamma_{\mu} |e_{\mu}\rangle \langle e_{\mu}| \quad (1)$$

where γ_{μ} quantifies the loss in the cavity with index μ and $\{|e_{\mu}\rangle\}$ is the basis where H_0 is represented (mode space). For simplicity we will assume in the following that the losses are concentrated in a single cavity $\mu = \mu_0$.

The corresponding scattering set-up is realized by coupling the isolated system to M channels that extend to infinity, see Fig. 1. We assume that these leads are one-dimensional and described by a tight-binding Hamiltonian H_{leads} with matrix elements $(H_{\text{leads}})_{nm} = t_L \delta_{m,n\pm 1}$. They support propagating waves with a dispersion relation $E(k) = 2t_L \cos(k)$, where k is the wave vector and $t_L < 0$ (we set $t_L = -1$ below). We further assume that the cavities where the channels are attached are lossless.

The scattering properties of the network are described by the $M \times M$ scattering matrix S which connects incoming $|I\rangle$ to outgoing $|O\rangle$ wave amplitudes via the relation $|O\rangle = S|I\rangle$. It can be expressed in terms of the isolated

system Eq. (1) as

$$S(k, \gamma) = -\hat{1} + 2\iota \frac{\sin k}{t_L} W^T \frac{1}{H_{\text{eff}}(k, \gamma) - E(k)} W \quad (2)$$

where $\hat{1}$ is the $M \times M$ identity matrix and $E(k)$ is the energy of the incident plane wave [48]. The rectangular $N \times M$ matrix W contains the coupling between cavities and channels. We assume $W_{nm} = w\delta_{nm}$. The effective Hamiltonian is

$$H_{\text{eff}}(k, \gamma) = H(\gamma) + \frac{e^{\iota k}}{t_L} W W^T. \quad (3)$$

Due to the second term the effective Hamiltonian H_{eff} is not Hermitian even without internal losses i.e. $\gamma = 0$.

Absorption matrix and CPA conditions – For $\gamma = 0$ the scattering matrix is unitary, $S^\dagger S = \hat{1}$. For $\gamma \neq 0$, however, this relation is violated and we introduce the operator $A(k, \gamma) \equiv \hat{1} - S^\dagger(k, \gamma)S(k, \gamma) = A^\dagger$ as a measure of the total absorption occurring in the system. For networks with one lossy cavity, $A(k, \gamma)$ has $M - 1$ degenerate zero eigenvalues while the last eigenvalue is $0 \leq \alpha(k, \gamma) \leq 1$. When $\alpha(k, \gamma) = 0$ the system does not absorb energy, while $\alpha(k, \gamma) = 1$ indicates complete absorption, i.e., a CPA. This latter equation can be satisfied only for isolated pairs $(k_{\text{CPA}}, \gamma_{\text{CPA}})$ which are the object of our interest. Note that unlike scattering resonances, k_{CPA} is real since it has to support a propagating incoming wave in the attached leads.

The CPA condition $\alpha(k_{\text{CPA}}, \gamma_{\text{CPA}}) = 1$ is equivalent to a zero eigenvalue of the scattering matrix, $s_{\text{CPA}} \equiv s(k_{\text{CPA}}, \gamma_{\text{CPA}}) = 0$. The corresponding eigenvector $|I_{\text{CPA}}\rangle$ identifies the shape of the incident field which will generate interferences that trap the wave inside the structure leading to its complete absorption, $\langle I_{\text{CPA}} | S^\dagger(k_{\text{CPA}}, \gamma_{\text{CPA}}) S(k_{\text{CPA}}, \gamma_{\text{CPA}}) | I_{\text{CPA}} \rangle = 0$.

Evaluation of CPA's – A zero eigenvalue of the scattering matrix $S(k, \gamma)$ corresponds to a pole of its inverse matrix, which can be represented as $S^{-1}(k, \gamma) = S(-k, \gamma)$. Thus the poles are the solutions of $\zeta(k, \gamma) \equiv \det(H_{\text{eff}}(-k, \gamma) - E(k)) = 0$, where κ is complex in general, and the CPA's can be found numerically by searching for the real solutions of this equation, $\zeta(k_{\text{CPA}}, \gamma_{\text{CPA}}) = 0$. Typical examples of the κ -evolution as γ increases, are shown in Fig. 1.

We proceed with the theoretical evaluation of CPA points. We will assume that $w \ll t_L$. Let us first consider the relevant limit of weak losses $\gamma \ll t_L$. In this case $E(k, \gamma) \approx E_0(k) + \Delta E(k, \gamma)$ where $\Delta E(k, \gamma)$ can be found via first order perturbation theory. The unperturbed Hamiltonian is H_0 and we consider one particular eigenvalue $E^{(0)} \equiv E(k^{(0)})$ and the corresponding normalized eigenvector $|\Psi^{(0)}\rangle$, i.e. $H_0|\Psi^{(0)}\rangle = E^{(0)}|\Psi^{(0)}\rangle$. Straightforward first order perturbation theory, together

with the condition that k_{CPA} has to be real, leads to

$$\frac{\cos(k^{(0)})}{\cos(k_{\text{CPA}})} = 1 - \frac{1}{2} \left(\frac{w}{t_L} \right)^2 \sum_m |\Psi_m^{(0)}|^2$$

$$\gamma_{\text{CPA}} = \frac{1}{2} v_g(k_{\text{CPA}}) \left(\frac{w}{t_L} \right)^2 \frac{\sum_m |\Psi_m^{(0)}|^2}{|\Psi_{\mu_0}^{(0)}|^2} \quad (4)$$

where $v_g(k) \equiv \frac{\partial E(k)}{\partial k} = -2t_L \sin(k)$ is the group velocity of the incoming wave while $\Psi_m^{(0)}$ and $\Psi_{\mu_0}^{(0)}$ represent the components of the wave function $|\Psi^{(0)}\rangle$ at the sites m, μ_0 where the leads and the dissipation are placed respectively. In the limiting case of $M = 1$ the multichannel CPA condition Eq. (4) becomes identical with the critical coupling (CC) concept between input channel and loss. This is nothing else than the so-called impedance matching condition, which once expressed in terms of losses, indeed states that radiative and material losses must be equal [49, 50]. At the same time, this condition is noticeable similar to the lasing condition, on exchanging losses with gain [16].

The accuracy of the perturbative calculation Eq. (4) is further scrutinized via direct numerical evaluations of $(k_{\text{CPA}}, \gamma_{\text{CPA}})$. A comparison of the results is shown in Fig. 2. It is interesting to point out that although our calculations are applicable in the limit of weak coupling, nevertheless the agreement of the exact CPA points with the first order perturbation expressions Eq. (4) applies for w/t_L as high as 0.5.

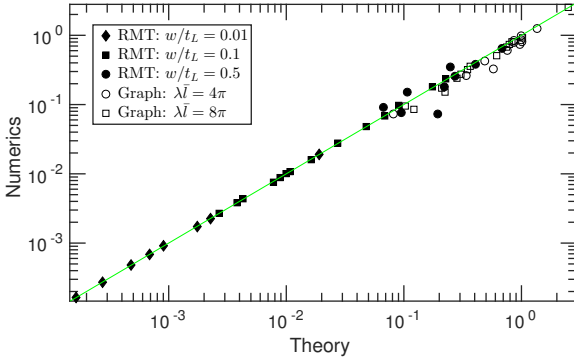


FIG. 2: (color online) Theoretical versus numerical values of $\gamma_{\text{CPA}}/v_g(k_{\text{CPA}})$ for various realizations of a complex network of $N = 15$ coupled resonators (filled symbols) and a tetrahedron graph (open symbols) respectively. Number of channels in both cases is $M = 3$ and TRI is preserved ($\beta = 1$). Various symbols correspond to different coupling constants w/t_L for the RMT model and vertex potentials for the graph.

Using Eq. (4) we can now provide a statistical description of the rescaled CPA $\tilde{\gamma}_{\text{CPA}} = 2 \left(\frac{t_L}{w} \right)^2 \frac{\gamma_{\text{CPA}}}{v_g(k_{\text{CPA}})} = \frac{\sum_m |\Psi_m^{(0)}|^2}{|\Psi_{\mu_0}^{(0)}|^2}$. The distribution $\mathcal{P}(\tilde{\gamma}_{\text{CPA}})$ can be easily calculated using the known results for the joint probability

distribution of the eigenfunction components $|\Psi_n^{(0)}|^2$ of a GOE (GUE) random matrix [30–32]. We get

$$\mathcal{P}_\beta(\tilde{\gamma}_{\text{CPA}}) = \mathcal{N}_\beta \frac{\tilde{\gamma}_{\text{CPA}}^{\beta \frac{M}{2} - 1}}{(1 + \tilde{\gamma}_{\text{CPA}})^{\beta \frac{M+1}{2}}} \quad (5)$$

where $\beta = 1(2)$ indicates an isolated system H_0 with preserved (violated) TRI. The normalization constants in front of the above distribution are $\mathcal{N}_1 = \frac{1}{\sqrt{\pi}} \frac{\Gamma(\frac{1+M}{2})}{\Gamma(\frac{M}{2})}$, $\mathcal{N}_2 = M$ and $\Gamma(x)$ is the gamma function [51].

From Eq. (5) we see that as the number of channels increases (the system becomes “more open”) a “statistical gap” is created that suppresses CPAs at small $\tilde{\gamma}$ (i.e. small γ or/and large velocities v_g) strengths. The “gap” is less pronounced when $\beta = 1$, since in this case weak localization interferences can support the trapping of the wave close to the lossy site. An estimation of the CPA gap, based on the $\tilde{\gamma}_{\text{CPA}}$ -value for which $\mathcal{P}(\tilde{\gamma}_{\text{CPA}})$ change curvature, leads to $\tilde{\gamma}_{\text{CPA}} \sim 0.1\beta M$ when $M \rightarrow \infty$.

A comparison of Eq. (5) with the numerical data for a complex network of $N = 15$ discs and $M = 1, 2, 3$ channels is shown in Fig. 3(a). A nice agreement is observed even though the coupling between the resonators and the leads has a moderate high value $w/t_L \approx 0.1$. For $\tilde{\gamma}_{\text{CPA}} \gg 1$ [56] the distribution Eq. (5) has a channel-independent power law shape $\mathcal{P}(\tilde{\gamma}_{\text{CPA}}) \sim 1/\tilde{\gamma}_{\text{CPA}}^{\beta+1}$. In the other limiting case $\tilde{\gamma}_{\text{CPA}} \ll 1$ we have $\mathcal{P}(\tilde{\gamma}_{\text{CPA}}) \sim \tilde{\gamma}_{\text{CPA}}^{\beta \frac{M}{2} - 1}$.

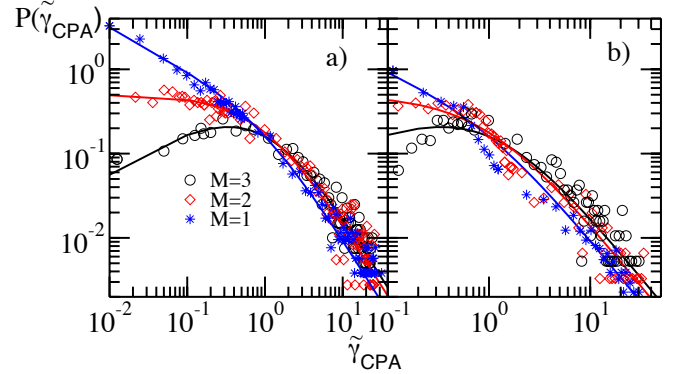


FIG. 3: (color online) (a) Distribution of the rescaled CPA $\tilde{\gamma}_{\text{CPA}}$ for a complex network of $N = 15$ cavities Eqs. (2,3). The numerical results are compared to the RMT prediction Eq. (5). (b) The same for a tetrahedron graph with $\lambda l = 4\pi$ at the vertices where the channels are attached. In both cases TRI is preserved, i.e. $\beta = 1$.

Let us now calculate the incident field which can lead to a CPA. Direct substitution of Eqs. (2), (3) in the definition of A allow us to re-write the absorption matrix in its spectral decomposition form:

$$A = -4\gamma \frac{\sin(k)}{t_L} |\alpha\rangle\langle\alpha|; \quad |\alpha\rangle = W^T \frac{1}{H_{\text{eff}}^\dagger - E(k)} |e_{\mu_0}\rangle. \quad (6)$$

From Eq. (6) it becomes obvious that the associated non-zero eigenvalue is $\alpha(k, \gamma) = -4\gamma \frac{\sin(k)}{t_L} \langle \alpha | \alpha \rangle$. Obviously the CPA incident waveform is given by the eigenvector $|\alpha(k_{\text{CPA}}, \gamma_{\text{CPA}})\rangle$. Using again first order perturbation theory we can write the incident field $|\alpha\rangle$ Eq. (6) associated with the non-degenerate eigenvalue $\alpha \neq 0$ of A in terms of the eigenvector $|\Psi^{(0)}\rangle$ of the isolated systems H_0 . Further substitution of $|\alpha(k_{\text{CPA}}, \gamma)\rangle$ and of k_{CPA} in Eq. (4) for the eigenvalue α gives:

$$\alpha(k_{\text{CPA}}; \gamma) = \frac{4\gamma/\gamma_{\text{CPA}}}{(1 + \gamma/\gamma_{\text{CPA}})^2} \quad (7)$$

which provides a simple expression of the relative absorption of the CPA cavity, at k_{CPA} , when $|I| \propto |\alpha(k_{\text{CPA}}, \gamma)|$. Eq. (7) dictates that the CPA sensitivity, defined as half-width-at-maximum, is proportional to γ_{CPA} . Similar analysis, when $\gamma = \gamma_{\text{CPA}}$, leads to the following expression for $\alpha(k; \gamma)$:

$$\alpha(k; \gamma_{\text{CPA}}) = u \cdot \frac{4v_g(k)/v_g(k_{\text{CPA}})}{(1 + v_g(k)/v_g(k_{\text{CPA}}))^2}. \quad (8)$$

Note that the second term in Eq. (8) has the same functional form as Eq. (7). The additional factor $u \equiv \left[1 + \frac{\cos^2 k^{(0)}}{(\cos k_{\text{CPA}} - \cos k^{(0)})^2} \tan^2\left(\frac{k - k_{\text{CPA}}}{2}\right)\right]^{-1}$ indicates that when $k_{\text{CPA}} \rightarrow k^{(0)}$ the absorption eigenvalue $\alpha(k; \gamma_{\text{CPA}})$ diminishes rapidly as k goes away from k_{CPA} .

We now consider the other limit of strong losses where many of the complex solutions of $\zeta(\kappa, \gamma) = 0$ turn back to the real axis and lead to a second CPA. The existence of CPAs for large γ is surprising since in the over-damping domain (i.e. large γ 's) it is expected to have strong reflections due to impedance mismatching. However, multiple interferences in complex systems provide a *zeroes self-trapping effect* which results in the CPAs. This is analogues to the well known resonant self-trapping phenomenon which has been thoroughly studied in other frameworks [52, 53] and it re-surface also in CPAs[54].

CPAs in Chaotic graphs – RMT addresses universal aspects of CPAs in complex systems. At the same time one needs to be aware that certain non-universal features (like scarring) may emerge when CPA cavities with underlying chaotic dynamics are considered. These features might influence the formation of CPAs. Therefore we test our theory with a model system, where such effects are known to be prominent, namely quantum graphs (networks of 1D waveguides) [37, 38, 40].

A graph consists of $n = 1, \dots, V$ vertices connected by bonds. The number of bonds emanating from a vertex n is its valency v_n and the total number of directed bonds (i.e. discerning $b \equiv n \rightarrow m$ and $\bar{b} \equiv m \rightarrow n$) is $2B = \sum_n^V v_n$. The length of each bond $l_b = l_{\bar{b}}$ is given by a box distribution centered around some mean value \bar{l} i.e. $l_b \in [\bar{l} - W_b/2, \bar{l} + W_b/2]$. The waves on the

bonds satisfy the Helmholtz equation $\frac{d^2 \Psi_b}{dx_b^2} + k^2 \Psi_b = 0$ (where $k > 0$ is the wavenumber). At the vertices the wavefunction is continuous and satisfies the relation $\sum_{b=1}^{v_n} d\Psi_b/dx_b|_{x_b=0} = \lambda_n \Psi_b(0)$. The parameters λ_n represents a potential concentrated on a vertex and for a lossy vertex it includes a negative imaginary part $-\iota\gamma_n$. We will restrict the losses to a single vertex μ_0 with a purely imaginary potential $-\iota\gamma$. Leads are attached to some of the remaining vertices $m = 1, \dots, M < V$, thus changing their valency to $\tilde{v}_m = v_m + 1$. The details for calculating the $M \times M$ scattering matrix for this system can be found in [38]. It can be represented in the form

$$S = S_{MM} + S_{MB} (\hat{1} - S_{BB})^{-1} S_{BM} \quad (9)$$

where the $2B \times 2B$ bond-scattering matrix $S_{BB}(k, \gamma)$ describes the multiple scattering and absorption inside the network, while the other three blocks account for direct scattering processes and the coupling between the leads and the network. We follow exactly the same program as for the RMT modeling and calculate the zeros of the S -matrix by evaluating the poles of its inverse $S^{-1}(k, \gamma) = S(-k, \gamma)$, i.e. by searching for the real solutions of the secular equation $\zeta(\kappa, \gamma) \equiv \det(\hat{1} - S_{BB}(-\kappa, \gamma)) = 0$. Our numerical data for the case of a fully connected tetrahedron, with one lossy vertex and $M = 1, 2$ and 3 leads attached to the other vertices are shown in Fig. 1b and demonstrate the same qualitative features as for the RMT model. Also the analytical evaluation of the CPA points via first-order perturbation theory parallels the RMT calculation and leads to the expression

$$\frac{\gamma_{\text{CPA}}}{v_g(k_{\text{CPA}})} = \frac{1}{2} \frac{\sum_m |\Psi_m^{(0)}|^2}{|\Psi_{\mu_0}^{(0)}|^2}; \quad k_{\text{CPA}} \approx k^{(0)} \quad (10)$$

where $\Psi_m^{(0)}$ and $\Psi_{\mu_0}^{(0)}$ denote the values of the unperturbed wave function at the vertices with attached leads and the lossy vertex, respectively, and the group velocity for the graphs is $v_g = \partial E / \partial k = 2k$ [37]. The universality of this expression can be further appreciated by realizing its similarity with Eq. (4) derived in the RMT framework. Eq. (10) has been checked against numerically evaluated CPA values for a tetrahedron graph, see Fig. 2.

Finally we have calculated numerically the distribution of $\tilde{\gamma}_{\text{CPA}} \equiv 2\gamma_{\text{CPA}}/v_g(k_{\text{CPA}})$ for graphs. The results for $M = 1, 2, 3$ and $\lambda\bar{l} = 4\pi$ are shown in Fig. 3(b) and are compared with the predictions of RMT Eq. (5). Clearly, our theory is capable of reproducing the main features of the distribution also for this model, where prominent scarring effects are known to exist [39, 40]. However, the agreement with Eq. (5) is less convincing for strong coupling to the leads ($\lambda = 0$, not shown) where a non-perturbative approach is necessary.

Conclusions - We investigated the distribution of loss-strengths for the realization of a chaotic CPA using a

RMT formalism. In the case of d absorbers one gets a distribution with power law tails that might even (e.g. for $d = 1$) not possess a mean value. This has to be contrasted to the case of uniform losses where one ends up with a χ^2 -distribution with exponentially decaying tails and well-defined mean. Furthermore for non-uniform losses we have discovered the novel effect of *zeroes self-trapping* which is absent for uniform losses. Finally we evaluated the robustness of CPA with respect to loss-detuning and we found that in case of frequency-detuning the upper bound for CPA robustness is controlled by the mean level spacing. The effects of semiclassical features, like scarring etc, are a subject of ongoing research.

Acknowledgement - (H.L, S.S. and T.K) acknowledge support from an AFOSR MURI grant FA9550-14-1-0037.

-
- [1] J. Mei *et al.*, Nature Comm. **3**, 756 (2012).
 - [2] G. Ma, M. Yang, S. Xiao, Z. Yang, P. Sheng, Nature Mater. **13**, 873 (2014).
 - [3] J. Z. Song, P. Bai, Z. H. hang, Y. Lai, N. J. Phys. **16**, 033026 (2014).
 - [4] V. Romero-Garcia, G. Theocharis, O. Richoux, A. Merkel, V. Tournat, V. Pagneux, Sci. Rep. **6**, 19519 (2016).
 - [5] F. Costa, S. Genovesi, A. Monorchio, G. Manara, IEEE Trans. Antennas Propag. **61**, 1201 (2013).
 - [6] Y. Pang, H. Cheng, Y. Zhou, J. Wang, J. Appl. Phys. **113**, 114902 (2013).
 - [7] J. Schindler, Z. Lin, J. M. Lee, H. Ramezani, F. M. Ellis, T. Kottos, J. Phys. A: Math. and Theor. **45**, 444029 (2012).
 - [8] W. Dallenbach, W. Kleinstaubler, Hochfrequenztechnik und Elektroakustik **51**, 152 (1938).
 - [9] W. W. Salisbury, U.S. Patent No. 2,599,944, 10 June (1952).
 - [10] J. Slater, *Microwave Electronics*, (Van Nostrand, Princeton, 1950).
 - [11] N. I. Landy, S. Sajuyigbe, J. J. Mock, D. R. Smith, W. J. Padilla, Phys. Rev. Lett. **100**, 207402 (2008).
 - [12] W. Padilla, X. Liu, SPIE Newsroom (2010).
 - [13] V. T. Pham, J. W. Park, D. L. Vu, H. Y. Zheng, J. Y. Rhee, K. W. Kim, Y. P. Lee, Adv. Nat. Sci. Nanosci. nanotechnol. **4**, 015001 (2013).
 - [14] C. M. Watts, X. Liu, W. J. Padilla, Adv. Lett. **24**, OP98 (2012).
 - [15] G. Dayal, S. A. Ramakrishna, Opt. Express **20**, 17503 (2012).
 - [16] Y. D. Chong, L. Ge, H. Cao, A. D. Stone, Phys. Rev. Lett. **105**, 053901 (2010).
 - [17] S. Longhi, Physics **3**, 61 (2010).
 - [18] W. Wan, Y. Chong, L. Ge, H. Noh, A. D. Stone, H. Cao, Science **331**, 889 (2011).
 - [19] Y. D. Chong, A. D. Stone, Phys. Rev. Lett. **107**, 163901 (2011).
 - [20] J. F. Zhang, K. F. Macdonald and N. I. Zheludev, Light: Science and Appl. **1**, 18 (2012).
 - [21] J. R. Piper, S. Fan, ACS Photonics **1**, 347 (2014).
 - [22] O. Kotlicki, J. Scheuer, Opt. Lett. **39**, 6624 (2014).
 - [23] Y. Sun, W. Tan, H.-q. Li, J. Li, H. Chen, Phys. Rev. Lett. **112**, 143903 (2014).
 - [24] M. L. Villinger, M. Bayat, L. N. Pye, A. Abouraddy, Opt. Lett. **40**, 5550 (2015).
 - [25] L. Baldacci, S. Zanotto, and A. Tredicucci, Rend. Fis. Acc. Lincei **26**, 219 (2015).
 - [26] B. C. P. Sturmberg, T. K. Chong, D-Y Choi, T. P. White, L. C. Botten, K. B. Dossou, C. G. Poulton, K. R. Catchpole, R. C. McPhedran, C. M. de Sterke, Optica **3**, 556 (2016).
 - [27] I. M. Vellekoop, A. Lagendijk, A. P. Mosk, Nature Photonics **4**, 320 (2010).
 - [28] Z. Yaqoob, D. Psaltis, M. S. Feld, C. Yang, Nat. Photon. **2**, 110 (2008).
 - [29] I. M. Vellekoop, A. P. Mosk, Opt. Lett. **32**, 2309 (2007).
 - [30] G. Akemann, J. Baik, and P. Di Francesco, eds., *The Oxford Handbook of Random Matrix Theory* (Oxford University Press, Oxford, 2010).
 - [31] H. J. Stockmann, *Quantum Chaos : An Introduction* (Cambridge University Press, Cambridge, 1999).
 - [32] C. W. J. Beenakker, Rev. Mod. Phys. **69**, 731 (1997).
 - [33] Y. Alhassid, Rev. Mod. Phys. **72**, 895 (2000).
 - [34] F. Evers and A. D. Mirlin, Rev. Mod. Phys. **80**, 1355 (2008).
 - [35] Y. V. Fyodorov, H-J Sommers, J. Math. Phys. **38**, 1918 (1997).
 - [36] H. Schomerus, Lecture notes, Les Houches Summer School “Stochastic Processes and Random Matrices”, (2015); arXiv:1610.05816.
 - [37] T. Kottos, U. Smilansky, Phys. Rev. Lett. **79**, 4794 (1997).
 - [38] T. Kottos, U. Smilansky, Phys. Rev. Lett. **85**, 968 (2000).
 - [39] S. Gnutzmann, H. Schanz and U. Smilansky. Phys. Rev. Lett. **110**, 094101 (2013).
 - [40] H. Schanz, T. Kottos, Phys. Rev. Lett. **90**, 234101 (2003).
 - [41] M. Bialous, V. Yunko, S. Bauch, M. Lawniczak, B. Dietz, L. Sirko, Phys. Rev. Lett. **117**, 144101 (2016).
 - [42] O. Hul, M. Lawniczak, S. Bauch, A. Sawicki, M. Kus, L. Sirko, Phys. Rev. Lett. **109**, 040402 (2012).
 - [43] O. Hul, S. Bauch, P. Pakonski, N. Savitskiy, K. Zyczkowski, and L. Sirko, Phys. Rev. E **69**, 056205 (2004).
 - [44] M. Allgaier, S. Gehler, S. Barkhofen, H.-J. Stöckmann, U. Kuhl, Phys. Rev. E **89**, 022925 (2014).
 - [45] J. Böhm, U. Kuhl, arXiv:1607.01221.
 - [46] J. D. Joannopoulos, S. G. Johnson, J. N. Winn, R. D. Meade, *Photonic Crystals: Molding the Flow of Light* 2nd ed. (Princeton University Press, Princeton, NJ, 2008).
 - [47] J. M. Lee, S. Factor, Z. Lin, I. Vitebskiy, F. M. Ellis, T. Kottos, Phys. Rev. Lett. **112**, 253902 (2014).
 - [48] S. Datta, *Electronic Transport in Mesoscopic Systems* (Cambridge University Press, Cambridge, U.K., 1995).
 - [49] H. A. Haus, *Waves and fields in optoelectronics*, Prentice-Hall, Englewood Cliffs, (1984).
 - [50] A. Yariv, P. Yeh, *Optical Electronics in Modern Communication*, Oxford University Press, New York (2007).
 - [51] Eq. (5) can be extended to the case of d equal absorbers (none of which are placed at the resonators coupled to the leads) leading to $\mathcal{P}_\beta(\tilde{\gamma}_{\text{CPA}}) = \tilde{\mathcal{N}}_\beta \frac{\tilde{\gamma}_{\text{CPA}}^{\beta \frac{M}{2} - 1}}{(1 + \tilde{\gamma}_{\text{CPA}})^{\beta \frac{M+d}{2}}}$ where $\tilde{\mathcal{N}}_\beta = \frac{\Gamma(\beta \frac{M+d}{2})}{\Gamma(\beta \frac{d}{2}) \Gamma(\beta \frac{M}{2})}$.
 - [52] J. Okolowicz, M. Płoszajczak, I. Rotter, **374**, 271 (2003).

- [53] V. V. Sokolov and V. G. Zelevinsky, **504**, Nucl. Phys. A **504** 562 (1989).
- [54] The applicability of RMT to the “super-radiance” CPA domain implies that other similar (in spirit) effects like super-resolution etc might also benefit from such approach.
- [55] In our simulations the matrix elements H_{nm}^0 (or their real and imaginary part for the GUE) are taken from a box distribution $[-W_{H_0}; W_{H_0}]$ rather than a Gaussian distribution.

In the large N limit, there is no significant difference between spectrum and eigenstates of this ensemble and the standard GOE/GUE ensemble. The density of states of H_0 is semi-circle with radius $R = W_{H_0}^2 \sqrt{N}/3$ and mean level spacing $\Delta \sim W_{H_0}^2 / \sqrt{N}$.

[56] For very large values of $\tilde{\gamma}_{\text{CPA}}$ the perturbative approach does not apply.

Supplemental Materials

We have checked numerically the validity of the theoretical predictions Eqs. (7,8) of the main text about the sensitivity of the CPA to wavenumber k and loss-strength γ detuning. To this end we have used an RMT model with one absorber and evaluated the eigenvalues of the absorption matrix. In this case there is at most one non-zero eigenvalue α . In Fig. S1 we report the behavior of α versus k and γ for a system of two channels $M = 2$. The peak indicates the position of $k_{\text{CPA}}, \gamma_{\text{CPA}}$. The blue continuous and black dashed lines indicate the theoretical predictions of Eqs. (7) and (8) respectively.

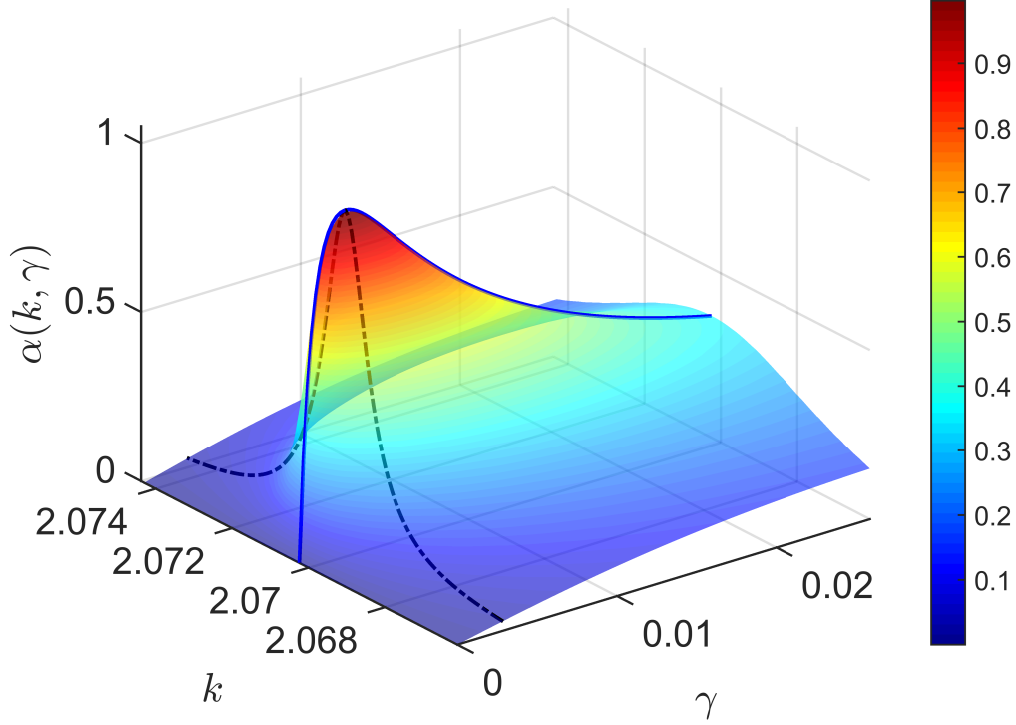


FIG. S1: (color online) The non-zero absorption eigenvalue $\alpha(k, \gamma)$ versus the wavenumber k and the loss-strength γ for a RMT system of $N = 5$ sites and two channels, with one lossy site in the middle (see inset of Fig. 1). The blue continuous and black dashed lines indicate the theoretical predictions of Eqs. (7) and (8) respectively.